J|A|C|S
ARTICLES

Published on Web 09/02/2010

# Rational Design of FRET-Based Ratiometric Chemosensors for in Vitro and in Cell Fluorescence Analyses of Nucleoside Polyphosphates

Yasutaka Kurishita,[†] Takahiro Kohira,[†] Akio Ojida,*[,‡] and Itaru Hamachi*[,†,§]

*Department of Synthetic Chemistry and Biological Chemistry, Graduate School of Engineering, Kyoto University, Katsura Campus, Nishikyo-ku, Kyoto 615-8510, Japan, Faculty of Pharmaceutical Sciences, Graduate School of Pharmaceutical Sciences, Kyushu University, 3-1-1 Maidashi, Higashi-ku, Fukuoka 812-8582, Japan, and CREST (Creation of Next-Generation Nanosystems through Process Integration), JST, Sanban-cho, Chiyoda-ku, Tokyo 102-0075, Japan*

Received April 28, 2010; E-mail: ojida@phar.kyushu-u.ac.jp; ihamachi@sbchem.kyoto-u.c.jp

***Abstract:*** Ratiometric fluorescence sensing is a useful technique for the precise and quantitative analysis of biological events occurring under complex conditions, such as those inside cells. We report herein the design of new ratiometric chemosensors for nucleoside polyphosphates such as ATP that are based on binding-induced modulation of fluorescence resonance energy transfer (FRET) coupled with a turn-on fluorescence-sensing mechanism. We designed these new FRET-based ratiometric chemosensors by utilizing spectral overlap changes to modulate the FRET efficiency. Introduction of coumarin fluorophores as the FRET donors into a binuclear zinc complex as the FRET acceptor provided the ratiometric chemosensors. These chemosensors exhibited a clear dual-mission signal change upon binding with strong affinity ($K_{app} \approx 10^6-10^7$ $M^{-1}$) to nucleoside polyphosphates in aqueous solution, whereas no detectable emission change was observed with monophosphates and phosphodiester species or various other anions. These chemosensors were used for real-time fluorescence monitoring of enzyme reactions such as saccharide synthesis by glycosyltransferase and phosphorylation by protein kinase, both of which involve nucleoside polyphosphates as substrates. The utility of ratiometric sensing by chemosensors was further demonstrated in a fluorescence-imaging study of the nucleoside polyphosphates inside living cells, wherein we ratiometrically visualized the stimulus-responsive concentration change of ATP, an indicator of the cellular energy level.

## Introduction

Fluorescence detection is an indispensable technique for the analysis of a variety of biological phenomena. During the past few decades, a number of small-molecule fluorescent chemosensors have been developed for use in biological analyses, which typically are elaborately designed to selectively detect a target substance or phenomenon.[1] Most chemosensors employ a single increase or decrease in their emission intensity as a sensing signal that responds to the target analyte(s). However, a fluorescence signal is readily perturbed by environmental factors, such as pH, temperature, and solvent polarity. Consequently, single-emission detection is sometimes problematic for precise fluorometrical analyses under biological conditions. In addition, *in cell* bioimaging studies by fluorescence microscopy using chemosensors as fluorescent probes suffer from their unknown concentration and inhomogeneous location inside the cells, which make it difficult to handle the fluorescence signal in a quantitative manner. Ratiometric measurement was devised to circumvent these unfavorable effects.[2] Ratiometric sensing involves the simultaneous measurement of two fluorescence signals at different wavelengths followed by calculation of their intensity ratio. This measurement eliminates the above-mentioned adverse effects on fluorescence signals and gives greater precision to the data analysis relative to single-channel detection.

Several sensing mechanisms have been exploited to realize ratiometric detection using two different fluorescence signals. One of the most representative mechanisms is coordination-induced fluorescence modulation, which has been widely adopted in the design of metal cation chemosensors.[3] For example, a ratiometric $Ca^{2+}$ sensor, such as fura-2, exhibits a wavelength shift in its excitation spectrum upon binding to $Ca^{2+}$ due to coordination-induced modulation of internal charge transfer (ICT).[2] However, this sensing mechanism, coupled with

[†] Kyoto University.
[‡] Kyushu University.
[§] CREST, JST.

(1) (a) *Advanced Concepts in Fluorescence Sensing, Part A: Small Molecule Sensing*; Geddes, C. D., Lakowicz, J. R., Eds.; Topics in Fluorescence Spectroscopy, Vol. 9; Springer: New York, 2005. (b) *Advanced Concepts in Fluorescence Sensing, Part B: Macromolecular Sensing*; Geddes, C. D., Lakowicz, J. R., Eds.; Topics in Fluorescence Spectroscopy, Vol. 10; Springer: New York, 2005.

(2) Grynkiewwicz, G.; Poenie, M.; Tsien, R. Y. *J. Biol. Chem.* **1985**, *260*, 3440.

(3) (a) Valeur, B.; Leray, I. *Coord. Chem. Rev.* **2000**, *205*, 3. (b) Haugland, R. P. *Guide to Fluorescent Probes and Labeling Techniques*; Invitrogen: Carlsbad, CA, 2005; Chapter 19. (c) Domaille, D. W.; Que, E. L.; Chang, C. J. *Nat. Chem. Biol.* **2008**, *4*, 168. (d) Kikuchi, K.; Komatsu, K.; Nagano, T. *Curr. Opin. Chem. Biol.* **2004**, *8*, 182.

 **10.1021/ja103615z** 

metal coordination, is not generally applicable for the detection of other substances such as anions or organic biomolecules. Another sensing mechanism that has been widely adopted in ratiometric detection is binding-induced modulation of fluorescence resonance energy transfer (FRET). Because of its facile control as a sensing mode and its basis on established theory,[5] FRET has been employed as a primary strategy in the design of protein-based biosensors using a pair of fluorescent proteins, such as the cyan fluorescent protein (CFP)−yellow fluorescent protein (YFP) pair.[4] In these biosensors, changes in distance and/or relative orientation of the two fluorescent proteins are the main factors that modulate the FRET efficiency. However, a similar FRET system cannot be readily built into small chemosensors because their fast rotational motion and small molecular size (i.e., smaller than the Förster distance) prohibit them from effectively modulating the FRET efficiency.[5] Therefore, the design of FRET-based dual-emission chemosensors remains a challenging task in the field of bioanalytical chemistry.

Among biological anions, nucleoside polyphosphates such as ATP play pivotal roles in various cellular events, both as the ubiquitous energy currency in all living organisms and as activated substrates in many enzymatic processes. Therefore, selective detection of these polyphosphate species under biological conditions would help elucidate their roles and related physiological events. In recent decades, a number of fluorescent chemosensors for nucleoside polyphosphates have been reported.[6,7] However, despite significant effort, there are few chemosensors capable of ratiometric detection of nucleoside polyphosphates.[6b−e] We recently developed a binuclear zinc complex as a fluorescent chemosensor that displays a turn-on single-emission change upon binding to nucleoside polyphosphates.[8] Herein, we report the design of new FRET-based ratiometric chemosensors for nucleoside polyphosphates that are based on the coupling of two sensing mechanisms, namely, turn-on fluorescence sensing and binding-induced modulation of FRET. We utilized spectral overlap changes as a modulation factor of FRET efficiency, in lieu of changes in distance or orientation of the fluorophores.[9] Introduction of coumarin fluorophores as the FRET donors into the binuclear zinc complex, which functions as the FRET acceptor, provides the ratiometric chemosensors, which exhibit a clear dual-emission signal change upon binding to nucleoside polyphosphates in aqueous solution. Taking advantage of this dual-sensing mode, we successfully applied the chemosensors to various biological analyses involving real-time fluorescence monitoring of enzyme reactions and ratiometric visualization of nucleoside polyphosphates in living cells.

## Results and Discussion

**Molecular Design and Synthesis.** We recently developed the binuclear Zn(II) complex **1**-2Zn(II) (Figure 1) as a selective fluorescent chemosensor for nucleoside polyphosphates.[8,10] **1**-2Zn(II) displays an large off−on-type fluorescence enhancement (33-fold) upon binding to ATP with strong affinity ($K_{app} = 1.3 \times 10^6$ $M^{-1}$) under neutral aqueous conditions. The mechanism of the fluorescence enhancement involves binding-induced recovery of the fluorescent conjugated form of the xanthene ring from its nonfluorescent nonconjugated state, which is formed by nucleophilic attack of zinc-bound water. We planned to exploit this sensing mode to design a FRET-based dual-emission chemosensor for nucleoside polyphosphates. The newly designed ratiometric chemosensors, **2**-2Zn(II) and **3**-2Zn(II), are shown in Figure 1. These chemosensors possess a coumarin unit, the FRET donor, that is connected to a xanthene ring, the FRET acceptor, through a short, rigid linker unit. In the nonbinding state, the xanthene part of the chemosensor adopts a nonconjugated form, so the chemosensors predominantly show blue emission from the coumarin unit (Figure 2). This is the case because the FRET is greatly suppressed by the minimal spectral overlap between the coumarin emission and the rather weak xanthene absorption ($\varepsilon < 3000$ $M^{-1}$ $cm^{-1}$).[8] The binding of a nucleoside polyphosphate induces recovery of the conjugated structure of the xanthene ring. This structural change brings about large spectral overlap between the two fluorophores, causing the chemosensors to exhibit strong green emission from the xanthene due to the significant enhancement of the FRET efficiency.

The strategy for synthesizing the dual-emission chemosensors is shown in Scheme 1. The Mannich-type reaction of **1** with 2-chloro-*N*-(hydroxymethyl)acetamide under acidic conditions gave **6**, which possesses an α-chloroacetamidomethyl group at the C5 position.[11] The substitution site was unambiguously determined by NMR spectroscopy: the C2 and C7 protons (7.03 and 6.87 ppm) were indentified by their clear NOE signals with the methylene protons of the two 2,2′-dipicolylamine (Dpa)

(4) (a) Frommer, W. B.; Davidson, M. W.; Campbell, R. E. *Chem. Soc. Rev.* **2009**, *38*, 2833. (b) VanEngelenburg, S. B.; Palmer, A. E. *Curr. Opin. Chem. Biol.* **2008**, *12*, 60. (c) Zhang, J.; Campbell, R. E.; Ting, A. Y.; Tsien, R. Y. *Nat. Rev. Mol. Cell Biol.* **2002**, *3*, 906. (d) Pollok, B. A.; Heim, R. *Trends Cell Biol.* **1999**, *9*, 57.

(5) Lakowicz, J. R. *Principles of Fluorescence Spectroscopy*, 3rd ed.; Springer: New York, 2006.

(6) (a) Ishida, Y.; Inoue, M.; Inoue, T.; Ojida, A.; Hamachi, I. *Chem. Commun.* **2009**, 2848. (b) Xu, Z.; Singh, N. J.; Lim, J.; Pan, J.; Kim, H. N.; Park, S.; Kim, K. S.; Yoon, J. *J. Am. Chem. Soc.* **2009**, *131*, 15528. (c) Ojida, A.; Nonaka, H.; Miyahara, Y.; Tamaru, S.; Sada, K.; Hamachi, I. *Angew. Chem., Int. Ed.* **2006**, *45*, 5518. (d) Ojida, A.; Miyahara, Y.; Wongkongkatep, J.; Tamaru, S.; Sada, K.; Hamachi, I. *Chem.−Asian J.* **2006**, *1*, 555. (e) Mizukami, S.; Nagano, T.; Urano, Y.; Odani, A.; Kikuchi, K. *J. Am. Chem. Soc.* **2002**, *124*, 3920.

(7) (a) Moro, A. J.; Cywinski, P. J.; Körste, S.; Mohr, G. J. *Chem. Commun.* **2010**, *46*, 1085. (b) Rhee, H.-W.; Choi, S. J.; Yoo, S. H.; Jang, Y. O.; Park, H. H.; Pinto, R. M.; Cameselle, J. C.; Sandoval, F. J.; Roje, S.; Han, K.; Chung, D. S.; Suh, J.; Hong, J.-I. *J. Am. Chem. Soc.* **2009**, *131*, 10107. (c) Schäferling, M.; Wolfbeis, O. S. *Chem.−Eur. J.* **2007**, *13*, 4342. (d) Neelakandan, P. P.; Hariharan, M.; Ramaiah, D. *J. Am. Chem. Soc.* **2006**, *128*, 11334. (e) Kwon, J. Y.; Singh, N. J.; Kim, H. N.; Kim, S. K.; Kim, K. S.; Yoon, J. *J. Am. Chem. Soc.* **2004**, *126*, 8892. (f) Abe, H.; Mawatari, Y.; Teraoka, H.; Fuijimoto, K.; Inouye, M. *J. Org. Chem.* **2004**, *69*, 495–504. (g) Lee, D. H.; Kim, S. Y.; Hong, J.-I. *Angew. Chem., Int. Ed.* **2004**, *43*, 4777. (h) Fabbrizzi, L.; Marcotte, N.; Stomeo, F.; Taglietti, A. *Angew. Chem., Int. Ed.* **2002**, *41*, 3811. (i) Sancenón, F.; Descalzo, A. B.; Martínez-Máñez, R.; Miranda, M. A.; Soto, J. *Angew. Chem., Int. Ed.* **2001**, *40*, 2640. (j) Schneider, S. E.; O'Neil, S. N.; Anslyn, E. V. *J. Am. Chem. Soc.* **2000**, *122*, 542. (k) Hosseini, M. W.; Blacker, A. J.; Lehn, J.-M. *J. Am. Chem. Soc.* **1990**, *112*, 3896.

(8) Ojida, A.; Takashima, I.; Kohira, T.; Nonaka, H.; Hamachi, I. *J. Am. Chem. Soc.* **2008**, *130*, 12095.

(9) (a) Zhang, X.; Xiao, Y.; Qian, X. *Angew. Chem., Int. Ed.* **2008**, *47*, 8025. (b) Albers, A. E.; Okreglak, V. S.; Chang, C. J. *J. Am. Chem. Soc.* **2006**, *128*, 9640. (c) Woodroofe, C. C.; Lippard, S. J. *J. Am. Chem. Soc.* **2003**, *125*, 11458. (d) Takakusa, H.; Kikuchi, K.; Urano, Y.; Sakamoto, S.; Yamaguchi, K.; Nagano, T. *J. Am. Chem. Soc.* **2002**, *124*, 1653. (e) Takakusa, H.; Kikuchi, K.; Urano, Y.; Kojima, H.; Nagano, T. *Chem.−Eur. J.* **2003**, *9*, 1479.

(10) (a) Sakamoto, T.; Ojida, A.; Hamachi, I. *Chem. Commun.* **2009**, 141. (b) Ojida, A.; Hamachi, I. *Bull. Chem. Soc. Jpn.* **2006**, *79*, 35. (c) Ojida, A.; Inoue, M.; Mito-oka, Y.; Tsutsumi, H.; Sada, K.; Hamachi, I. *J. Am. Chem. Soc.* **2006**, *128*, 2052. (d) Ojida, A.; Mito-oka, Y.; Sada, K.; Hamachi, I. *J. Am. Chem. Soc.* **2004**, *126*, 2454. (e) Ojida, A.; Inoue, M.; Mito-oka, Y.; Hamachi, I. *J. Am. Chem. Soc.* **2003**, *125*, 10184. (f) Ojida, A.; Park, S.-K.; Mito-oka, Y.; Hamachi, I. *Tetrahedron Lett.* **2002**, *43*, 6193. (g) Ojida, A.; Mito-oka, Y.; Inoue, M.; Hamachi, I. *J. Am. Chem. Soc.* **2002**, *124*, 6256.

(11) Shipchandler, M. T.; Fino, J. R.; Klein, L. D.; Kirkemo, C. L. *Anal. Biochem.* **1987**, *162*, 89.

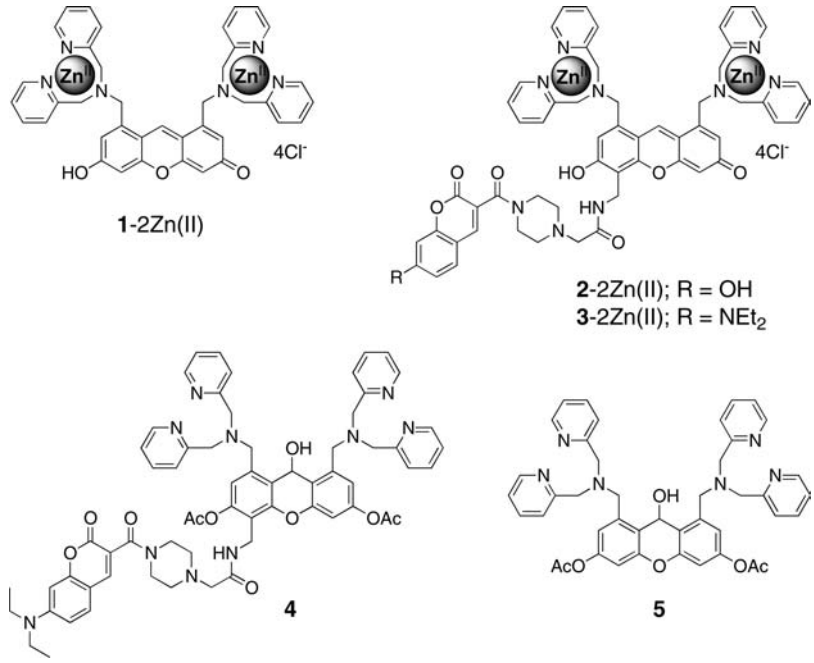


***Figure 1.*** Structures of the chemosensors.

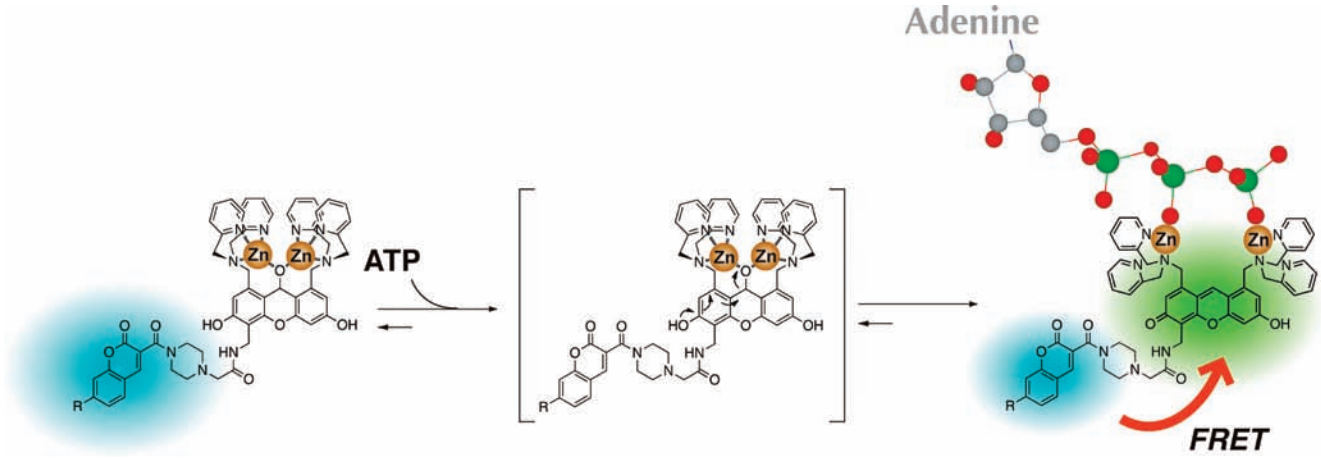


***Figure 2.*** Schematic illustration of the dual-emission sensing of ATP with the chemosensors. The chemosensors undergo FRET via a turn-on fluorescence-sensing mechanism.

units, and the C4 proton (6.68 ppm) was identified as a single peak that showed no NOE correlation with other proton peaks. The nucleophilic reaction of **6** with hydroxycoumarin derivative **7** gave ligand **2**, which was treated with 2 equiv of $ZnCl_2$ to yield the zinc complex **2**-2Zn(II) as a FRET-type chemosensor. Employing different types of coumarin allows control of the detection wavelength and emission ratio value. Thus, the chemosensor **3**-2Zn(II) was prepared by the same procedure via nucleophilic reaction of **6** with aminocoumarin derivative **8** followed by zinc complexation.

**Fluorescence Sensing of Phosphate Derivatives.** The spectroscopic analysis of ligand **2** was initially conducted in aqueous MeOH solution. The solution of **2** (5 $\mu$M) showed two distinct UV peaks at 341 and 513 nm, which correspond to the absorbance of the hydroxycoumarin and xanthene units, respectively. Upon titration with $ZnCl_2$, the absorbance at 513 nm decreased significantly and almost disappeared in the presence of 2 equiv of $ZnCl_2$, whereas the absorbance at 341 nm decreased only slightly (Figure 3a). The large decrease in absorption at 513 nm is comparable with that observed in **1**-2Zn(II),[8] indicating the formation of the 2:1 complex, which induces the disruption of the xanthene conjugate structure via attack of the zinc-bound water molecule. When the solution of ligand **2** was excited at 341 nm, distinct emissions due to the coumarin and xanthene units were observed at 454 and 525 nm, respectively (Figure 3b). This dual-emission spectrum significantly changed in a seesaw manner upon zinc titration. The large increase in emission at 454 nm and the concomitant decrease in emission at 525 nm strongly suggest that FRET from the coumarin unit to the xanthene unit is effectively canceled as a result of a decrease in the spectral overlap between the coumarin emission and the xanthene absorption (Figure S1 in the Supporting Information).

The fluorescence-sensing ability of zinc complex **2**-2Zn(II) toward nucleoside polyphosphates was evaluated under aqueous conditions (50 mM HEPES, 10 mM NaCl, 1 mM $MgCl_2$, pH 7.2). The fluorescence emission change of **2**-2Zn(II) (0.5 $\mu$M) upon addition of ATP (0−5 $\mu$M) is shown in Figure 4a.

***Scheme 1.*** Synthesis of Chemosensors **2**-2Zn(II) and **3**-2Zn(II)

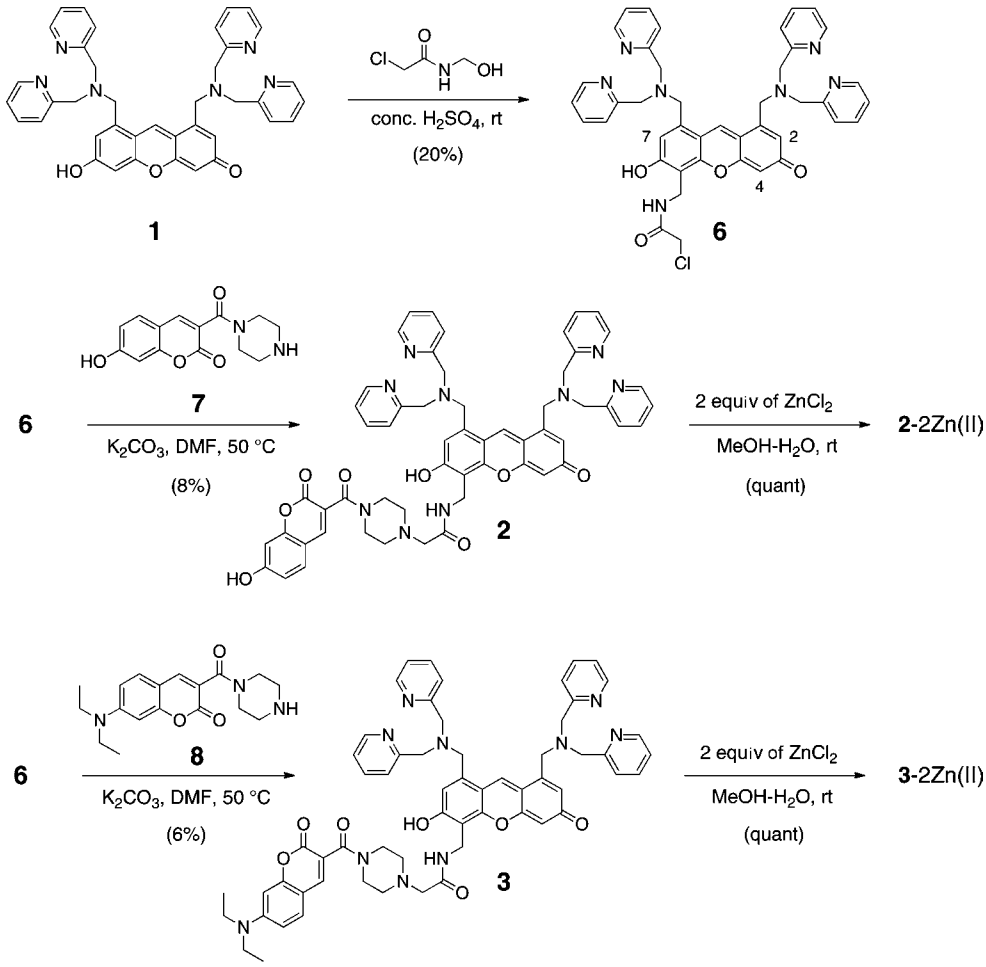


Excitation of the coumarin unit at 341 nm induced a clear seesaw-type dual-emission change, suggesting the recovery of FRET from the coumarin ($F_{max}$ at 454 nm) to the xanthene ($F_{max}$ at 525 nm) due to the recovery of spectral overlap between the coumarin emission and the xanthene absorption in the ATP-bound complex. The ratio $R$ of the emissions at the two wavelengths ($R = F_{xanthene}/F_{coumarin}$) increased from 0.14 to 1.95 ($\Delta R = 1.81$; Figure 4c), and the FRET efficiency of the ATP-bound complex of **2**-2Zn(II) was calculated to be 76%. As expected, direct excitation of the xanthene ring at 488 nm showed a large emission increase upon ATP addition, strongly supporting the conclusion that the conjugate structure of the xanthene ring was recovered. A plot of the fluorescence emission change ($F/F_0 - 1$) at 525 nm shows typical saturation behavior (Figure S2 in the Supporting Information); curve-fitting analysis provided an affinity constant ($K_{app}$) of $2.9 \times 10^6$ $M^{-1}$ for ATP. The fluorescence Job's plot revealed that their binding stoichiometry was 1:1 (Figure S3 in the Supporting Information). A similar dual-emission change was observed upon titration of **3**-2Zn(II) with ATP (Figure 4b): a decrease in the coumarin fluorescence ($F_{max}$ at 477 nm) and a concomitant large increase in the xanthene fluorescence ($F_{max}$ at 528 nm) were observed when the coumarin was excited at 414 nm. The increase in the emission ratio ($\Delta R = 7.51$) was larger than that observed for **2**-2Zn(II) ($\Delta R = 1.81$) (Figure 4c). This large $\Delta R$ is partially ascribed to the direct excitation of the regenerated fluorescent xanthene unit at 414 nm. The FRET efficiency of the ATP−**3**-2Zn(II) binding complex was determined to be 83%.

The sensing selectivity of the chemosensors for a variety of biologically relevant anions was examined by fluorescence titration experiments. The values of $K_{app}$ and $\Delta R$ for **2**-2Zn(II) upon addition of 10 equiv of various anions are summarized in Table 1. Chemosensor **2**-2Zn(II) shows strong binding affinity in the range $1.2 \times 10^6$ to $5.2 \times 10^6$ $M^{-1}$ toward various polyphosphate derivatives such as NTP (N = A, G, C), NDP (N = A, U), and inorganic pyrophosphate (PPi). The emission-ratio changes were in the range 1.4−1.7 for NTPs and 0.7 for NDPs. The largest $\Delta R$ was observed with inorganic pyrophosphate ($\Delta R = 4.7$). On the other hand, little fluorescence change was induced by monophosphate species such as AMP, $HPO_4^-$, c-GMP, c-AMP, ADP-Glu, and UDP-Gal and non-phosphate anions ($AcO^-$, $SO_4^{2-}$, $NO_3^-$, $HCO_3^-$). Chemosensor **3**-2Zn(II) also showed strong binding affinity and sensing selectivity toward polyphosphate species, comparable to those observed for **2**-2Zn(II) (Table 1). Importantly, **3**-2Zn(II) exhibited larger $\Delta R$ values than **2**-2Zn(II), in the range 4.9−7.5 for NTPs and 2.8−3.0 for NDPs. The largest $\Delta R$ was observed with PPi ($\Delta R = 15$). Overall, these results demonstrate that **2**-2Zn(II) and **3**-2Zn(II) are useful chemosensors that are capable of dual-emission detection of polyphosphates, have strong binding affinities, and exhibit useful ratiometric changes.

**Real-Time Fluorescence Monitoring of Enzyme Reactions.** Nucleoside polyphosphates are involved in many important enzyme reactions as key reactive substrates. Therefore, ratiometric fluorescent chemosensors selective for nucleoside polyphosphates would provide a general assay system for these

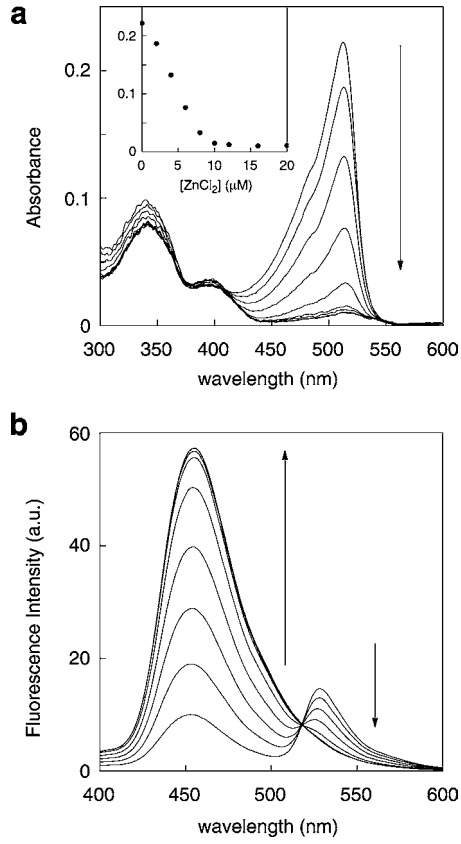


***Figure 3.*** (a) UV absorption and (b) fluorescence spectral change of ligand **2** upon addition of $ZnCl_2$ (1−20 $\mu$M). Inset: plot of UV absorbance at 513 nm upon zinc(II) titration. Measurement conditions: 5 $\mu$M **2** in 1:1 50 mM HEPES (pH 7.4)/MeOH, 25 °C, $\lambda_{ex}$ = 341 nm.

enzyme activities that has high sensitivity and accuracy. We applied the chemosensors to in vitro real-time monitoring of two enzyme reactions involving nucleoside polyphosphates: saccharide synthesis by glycosyltransferase and phosphorylation by protein kinase (Scheme 2).

In saccharide biosyntheses catalyzed by glycosyltransferase, a nucleotide sugar such as UDP glycoside predominantly serves as a sugar donor to form a new glycosyl bond with a glycosyl acceptor (Scheme 2). Since UDP is produced from UDP glycoside during a glycosyl transfer process, selective detection of the produced UDP in effect would monitor the saccharide synthesis without perturbing the sugar products. **2**-2Zn(II) can ratiometrically sense UDP with a high binding affinity but poorly detects UDP-Gal, as shown in Table 1. Therefore, we employed **2**-2Zn(II) to monitor the glycosyl transfer reaction between UDP-Gal and *N*-acetylglucosamine (GlcNAc) catalyzed by $\beta$-1,4-galactosyltransferase ($\beta$-1,4-GalT).[6d,12] As shown in Figure 5a, a clear ratiometric emission change due to the formation of UDP was observed during the reaction, in which the emission ratio ($R = F_{xanthene}/F_{coumarin}$) gradually increased in a time-dependent manner. The reaction rate was accelerated by increasing the concentration of GlcNAc. The Lineweaver−Burk plot gave a Michaelis constant ($K_m$) of 391 $\mu$M for GlcNAc (Figure 5b), which is very similar to the value reported previously (441 $\mu$M).[13]

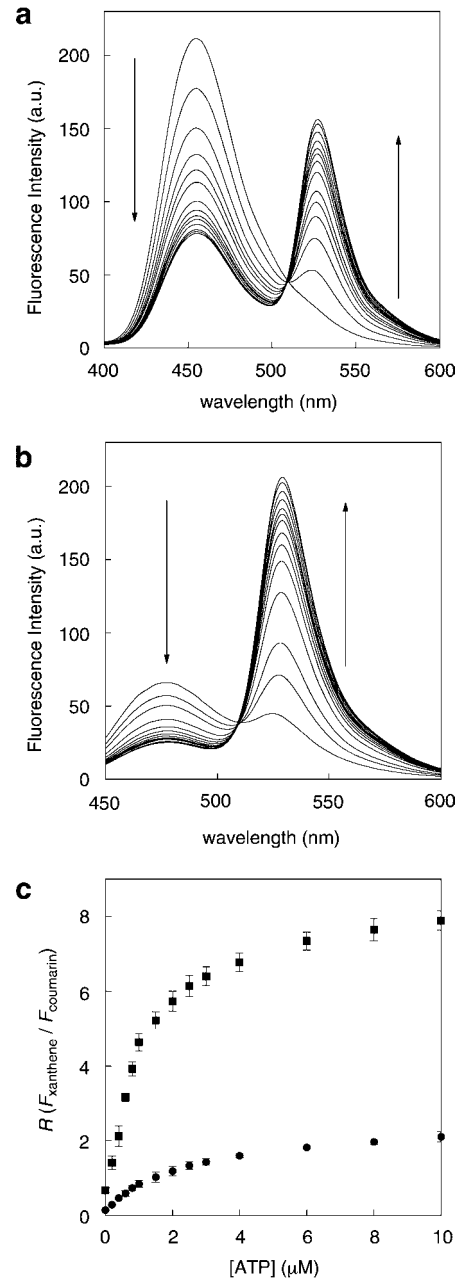


***Figure 4.*** Fluorescence spectral changes of (a) **2**-2Zn(II) and (b) **3**-2Zn(II) upon addition of ATP (0−5 $\mu$M). Measurement conditions: 0.5 $\mu$M **2**-2Zn(II) or **3**-2Zn(II) in 50 mM HEPES, 10 mM NaCl, 1 mM $MgCl_2$, pH 7.4, 25 °C, $\lambda_{ex}$ = (a) 341 and (b) 414 nm. (c) Plot of the emission ratio *R* upon ATP titration of **2**-2Zn(II) (●) and **3**-2Zn(II) (■), wherein *R* is defined as the ratio of the emission intensities at the two wavelengths [$F_{525nm}/F_{454nm}$ for **2**-2Zn(II) and $F_{528nm}/F_{477nm}$ for **3**-2Zn(II)].

A phosphorylation reaction catalyzed by protein kinase was also ratiometrically monitored using **3**-2Zn(II) (Scheme 2). In this assay, the phosphorylation reaction can be fluorescently traced by detecting the conversion of ATP to ADP. As shown in Table 1, **3**-2Zn(II) displays a large difference between the $\Delta R$ values for ATP and ADP, which can be utilized to quantify the change in ATP relative to ADP during the kinase-catalyzed phosphorylation process. The model system we used was the phosphorylation reaction of p-CREB peptide catalyzed by glycogen synthase kinase 3$\beta$ (GSK-3$\beta$).[14] The time-dependent

(12) (a) Kohira, T.; Takashima, I.; Nonaka, H.; Ojida, A.; Hamachi, I. *Chem. Lett.* **2008**, *37*, 1164. (b) Wongkongkatep, J.; Miyahara, Y.; Ojida, A.; Hamachi, I. *Angew. Chem., Int. Ed.* **2006**, *45*, 665.
(13) O'Keeffe, E. T.; Hill, R. L.; Bell, J. E. *Biochemistry* **1980**, *19*, 4954.
(14) Cohen, P.; Frame, S. *Nat. Rev. Mol. Cell Biol.* **2001**, *2*, 769.

***Table 1.*** Summary of the Apparent Binding Constants ($K_{app}$) for Binding to Various Anions and Corresponding Emission-Ratio Changes ($\Delta R$) for **2**-2Zn(II) and **3**-2Zn(II)[a]

| | **2**-2Zn(II) | | **3**-2Zn(II) | |
|---|---|---|---|---|
| anion species[b] | $K_{app}$ ($M^{-1}$) | $\Delta R$[d] | $K_{app}$ ($M^{-1}$) | $\Delta R$[d] |
| ATP | $2.9 \times 10^6$ | 1.8 | $7.3 \times 10^6$ | 7.5 |
| ADP | $3.6 \times 10^6$ | 0.7 | $6.6 \times 10^6$ | 3.0 |
| AMP | n.d.[c] | −[c] | n.d.[c] | −[c] |
| GTP | $2.0 \times 10^6$ | 1.8 | $4.5 \times 10^6$ | 7.1 |
| CTP | $1.4 \times 10^6$ | 1.4 | $3.3 \times 10^6$ | 4.9 |
| UDP | $1.2 \times 10^6$ | 0.7 | $1.8 \times 10^6$ | 2.8 |
| PPi | $5.2 \times 10^6$ | 4.7 | $1.3 \times 10^7$ | 15 |
| $HPO_4^{2-}$ | n.d.[c] | −[c] | n.d.[c] | −[c] |
| c-GMP | n.d.[c] | −[c] | n.d.[c] | −[c] |
| c-AMP | n.d.[c] | −[c] | n.d.[c] | −[c] |
| ADP-Glu | n.d.[c] | −[c] | n.d.[c] | −[c] |
| UDP-Gal | n.d.[c] | −[c] | n.d.[c] | −[c] |
| $AcO^-$ | n.d.[c] | −[c] | n.d.[c] | −[c] |
| $SO_4^{2-}$ | n.d.[c] | −[c] | n.d.[c] | −[c] |
| $NO_3^-$ | n.d.[c] | −[c] | n.d.[c] | −[c] |
| $HCO_3^-$ | n.d.[c] | −[c] | n.d.[c] | −[c] |

[a] Measurement conditions: 50 mM HEPES, 10 mM NaCl, 1 mM $MgCl_2$, pH 7.4, 25 °C, with $\lambda_{ex}$ = 341 nm for **2**-2Zn(II) and 414 nm for **3**-2Zn(II). [b] Abbreviations of the anions are defined in the Experimental Section. [c] Not determined because of the small fluorescence change. [d] $\Delta R$ indicates the change in the emission ratio $R$ in the presence of 10 equiv of anion relative to the value without anion.

emission change during the phosphorylation reaction is shown in Figure 6a. It is apparent that the emission ratio ($F_{xanthene}/F_{coumarin}$) gradually decreased with reaction time, which can be reasonably ascribed to the conversion of ATP to ADP as a result of the phosphorylation of p-CREB peptide. Indeed, the formation of the doubly phosphorylated peptide (2p-CREB) was confirmed by MALDI-TOF mass spectrometric analysis (data not shown). Kinetic analysis based on first-order reaction kinetics indicated that the initial rate of the reaction is proportional to the amount of GSK-3$\beta$ (Figure 6b).

Both glycosyltransferases and protein kinases are central enzymes in essential biological events, such as the biosyntheses of a wide variety of oligosaccharides and the control of a diverse range of cell-signaling events, respectively.[15] Therefore, these enzyme families are regarded as important targets in drug discovery.[16] The two assay systems described here do not require any special modification of the substrates, and thus should be generally useful not only for probing their enzyme activities but also for inhibitor screening.

**Ratiometric Analysis of Nucleoside Polyphosphates in Living Cells.** As mentioned above, the advantages of ratiometric detection can be effectively exploited under complicated biological conditions, such as those inside cells. We next applied the chemosensors to the ratiometric visualization of nucleoside polyphosphates in mammalian living cells. It is well-known that cells usually contain submicromolar to millimolar amounts of various nucleoside polyphosphates.[17] The most abundant is ATP, the average concentration of which in normal and tumor cells is 2.5 and 3.1 mM, respectively.[17] This concentration is outside the sensing range of the chemosensors for nucleoside polyphosphates (0.1−10 $\mu$M). However, it could be expected that the steady-state emission ratio $R$ would change depending on the relative amounts of N*T*Ps versus N*D*Ps, because the chemosensors exhibit distinct ratio values for these species (Table 1). To test this hypothesis, we initially evaluated the fluorescence response of **3**-2Zn(II) by changing the ATP concentration fraction, i.e., [ATP]/([ATP] + [ADP]), while maintaining a constant total concentration ([ATP] + [ADP] = 3 mM). This experiment was conducted in a solution of HEPES-buffered saline (107 mM NaCl, 6 mM KCl, 1.2 mM $MgSO_4$, 2 mM $CaCl_2$, 11.5 mM glucose, 20 mM HEPES, pH 7.4) supplemented with 3 mM glutathione, 3 mM inorganic phosphate, and 50 $\mu$M inorganic pyrophosphate in order to mimic cytosolic conditions.[17] As shown in Figure 7, the emission ratio $R$ of **3**-2Zn(II) changed from 7.3 to 12.2 as the ATP concentration fraction increased from 0.17 to 0.83. This result also clearly indicates that the binding equilibrium of **3**-2Zn(II) between two nucleoside polyphosphates operates even under high-concentration conditions, allowing changes in their relative concentration to be fluorescently detected using the emission ratio $R$.[18]

For the ratiometric detection of intracellular nucleoside polyphosphates, we employed the aminocoumarin-type chemosensor **3**-2Zn(II) because of its large emission-ratio response ($\Delta R$, Table 1) and less pH-sensitive fluorescence profile relative to **2**-2Zn(II) (Figure S5 in the Supporting Information). Since **3**-2Zn(II) itself does not penetrate the cell membrane, **3** was chemically modified by acetylation at both hydroxyl groups to increase its lipophilicity. The treatment of **3**-2Zn(II) with acetic anhydride in *N*,*N*-dimethylformamide (DMF) and subsequent HPLC purification under acidic conditions [0.1% trifluoroacetic acid (TFA)] gave the acetylated ligand **4**, which was used for the cell-imaging study following complexation with 2 equiv of $ZnCl_2$.

When HeLa cells were treated with the zinc(II) complex of **4** [**4**-2Zn(II)] at a concentration of 10 $\mu$M for 15 min in HBS buffer and then incubated for 60 min in DMEM, bright fluorescence of the xanthene unit was nearly uniformly observed inside the cells (Figure S6 in the Supporting Information). This indicates that the nonfluorescent **4**-2Zn(II) penetrated into the cells and that fluorescent **3**-2Zn(II) was subsequently formed by esterase-catalyzed hydrolysis of the acetyl groups and distributed throughout the cells. Pixel-by-pixel ratio images of the cells were obtained from two fluorescence images, one taken through the coumarin channel (470−500 nm) and the other through the xanthene channel (530−630 nm). A representative image (Figure 8a) shows that the ratio is not constant throughout the cell, implying that the nucleoside polyphosphates are not uniformly distributed inside the cells. To monitor the stimuli-responsive changes of the ATP level, the cells were treated with 2-deoxyglucose (2-DG) and/or potassium cyanide (KCN); these compounds inhibit ATP synthesis by disturbing glycolysis or oxidative phosphorylation, respectively. As shown in Figure 8a, a significant ratio change was observed after 60 min when ATP production was inhibited by these inhibitors. A large decrease in $R$ (xanthene channel/coumarin channel) is also evident from the time-lapse ratio images (Figure 8b) and the time-course plot

(15) Holemann, A.; Seeberger, P. H. *Curr. Opin. Biotechnol.* **2004**, *15*, 615.
(16) (a) Izumi, M.; Yuasa, H.; Hashimoto, H. *Curr. Top. Med. Chem.* **2009**, *9*, 87. (b) Hinou, H.; Nishimura, S. *Curr. Top. Med. Chem.* **2009**, *9*, 106. (c) Mazanetz, M. P.; Fischer, P. M. *Nat. Rev. Drug Discovery* **2007**, *6*, 464. (d) Cohen, P.; Goedert, M. *Nat. Rev. Drug Discovery* **2004**, *3*, 479.
(17) (a) Traut, T. W. *Mol. Cell. Biochem.* **1994**, *140*, 1. (b) Barshop, B. A.; Adamson, D. T.; Vallom, D. C.; Rosen, F.; Epstein, B. L.; Seegmiller, J. E. *Anal. Biochem.* **1991**, *197*, 266.

(18) We examined the sensing range of the chemosensor toward ATP in a solution of HEPES-buffered saline supplemented with 3 mM glutathione, 3 mM inorganic phosphate, and 50 $\mu$M inorganic pyrophosphate. The fluorescent titration data indicated that the sensing range was lowered to ~1 mM in this cytosol-like solution (Figure S4 in the Supporting Information).

***Scheme 2.*** Two Enzyme Reactions Involving Nucleoside Pyrophosphates Fluorescently Detected Using the Chemosensors

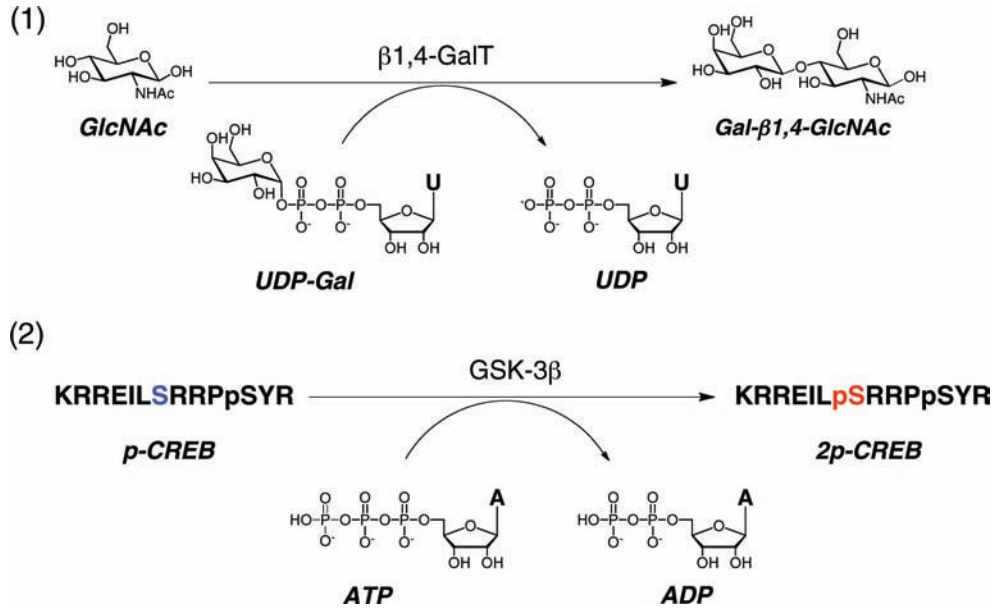


(Figure 8d). In contrast, in the control experiment, the ratio value scarcely changed during 60 min in the absence of the inhibitors (Figure 8c). Interestingly, treatment with 2-DG alone (20 mM) induced a moderate decrease in $R$ ($\Delta R = 0.32$), while KCN alone (1 mM) had almost no effect on $R$ (Figure 8d and Figure S7 in the Supporting Information). A larger decrease in $R$ ($\Delta R = 0.6$) was observed in the case of the combined treatment of cells with 2-DG (20 mM) and KCN (1 mM), as shown in Figure 8d. It is of particular importance that the time-dependent ratio changes induced by the three different stimuli are in good agreement with a recent report of ATP detection using a protein-

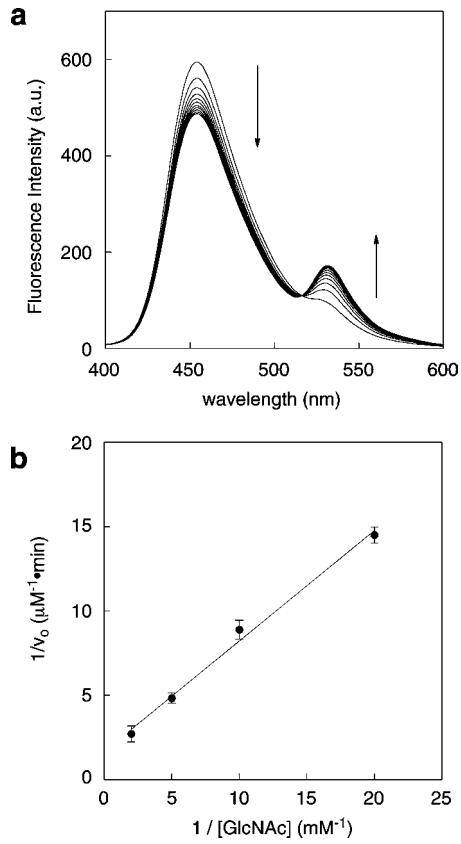


***Figure 5.*** Real-time fluorescence detection of the glycosyl transfer reaction catalyzed by $\beta$-1,4-GalT: (a) time trace (0−20 min) of the fluorescence spectral change of **2**-2Zn(II); (b) Lineweaver−Burk plot analysis of the enzyme reaction. The experimental conditions are described in the Experimental Section.

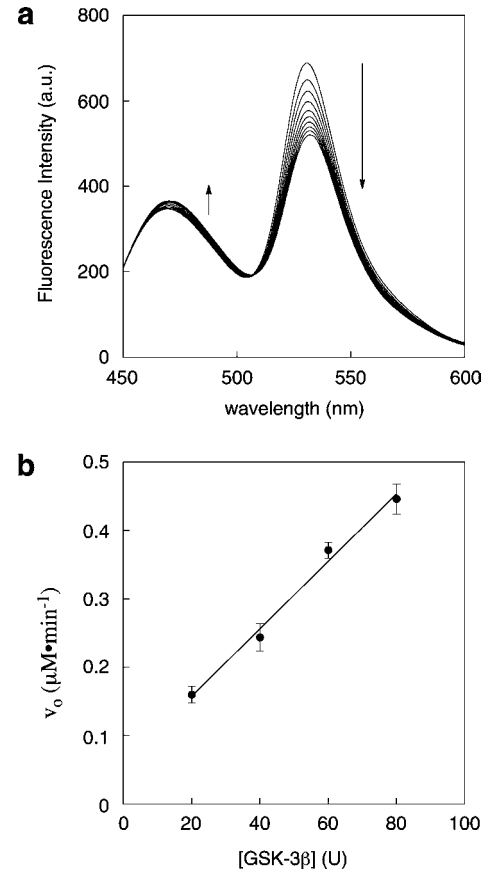


***Figure 6.*** Real-time fluorescence detection of the phosphorylation reaction catalyzed by GSK-3$\beta$: (a) time trace (0−180 min) of the fluorescence spectral change of **3**-2Zn(II); (b) plot of the initial rate ($v_0$, $\mu$M min$^{-1}$) as a function of the amount of GSK-3$\beta$. Detailed experimental conditions are described in the Experimental Section.

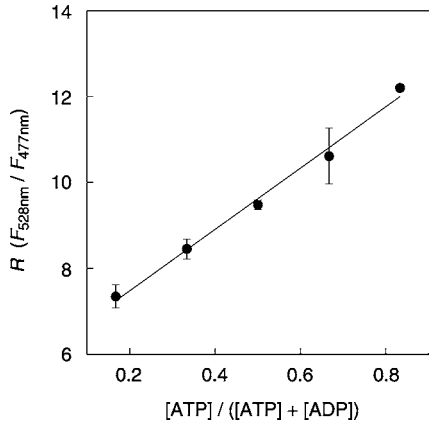


***Figure 7.*** Ratiometric fluorescence response of **3**-2Zn(II) obtained by changing the ATP concentration fraction at a constant total concentration of ATP and ADP. Measurement conditions: 10 $\mu$M **3**-2Zn(II), [ATP] + [ADP] = 3 mM, HEPES-buffered saline (107 mM NaCl, 6 mM KCl, 1.2 mM $MgSO_4$, 2 mM $CaCl_2$, 11.5 mM glucose, 20 mM HEPES, pH 7.4), 3 mM glutathione, 3 mM inorganic phosphate, 50 $\mu$M inorganic pyrophosphate, $\lambda_{ex}$ = 458 nm, 25 °C.

based fluorescent biosensor.[19] A second control experiment using ligand **4** without bound zinc showed only a subtle ratio change, even when both inhibitors were added (Figures S8 and S9 in the Supporting Information), suggesting that **4**-2Zn(II) exists as the zinc complex inside cells and that the complex detects concentration changes of ATP. It should also be noted that a comparable imaging study could not be accomplished with the zinc complex of **5**, which was converted to **1**-2Zn(II) inside the cells.[8] This is the case because the extremely heterogeneous localization of **1**-2Zn(II) inside the cells precluded quantitative analysis of ATP based on a single emission intensity (Figure S10 in the Supporting Information).

The ratiometric imaging was further conducted with other cell lines, such as HEK293 and NIH3T3 cells. The stimuli-responsive emission ratio changes of HEK293 cells are shown in Figure 8e and Figure S11 in the Supporting Information. Interestingly, the *R* value decreased significantly upon treatment not only with 2-DG (1 mM) alone but also with KCN (0.1 mM) alone. This response pattern is different than that for HeLa cells, which were almost insensitive to relatively high concentrations of KCN (1 mM). NIH3T3 cells also showed a large decrease in *R* in response to both inhibitors (Figure S12 in the Supporting Information). Such cell-line-dependent responses might be ascribed to differences in their metabolic pathways, namely, the fact that HeLa cells mainly depend on glycolysis for ATP synthesis while HEK293 and NIH3T3 cells employ both glycolysis and oxidative phosphorylation pathways.[20] In addition, the present results seem consistent with the fact that cancerous cells mainly depend on ATP synthesis through glycolysis rather than oxidative phosphorylation.[20] However, further metabolic analyses must be performed to precisely validate this hypothesis. The data also revealed that the combined treatment with 2-DG and KCN works more effectively to reduce the ATP level in HEK293 and NIH3T3 cells than treatment with 2-DG or KCN alone. Overall, the data indicate that **3**-2Zn(II) is a ratiometric chemosensor that can be used for sensing and imaging changes in ATP levels inside living cells, which in turn directly correlate with the cellular energy level.

(19) Imamura, H.; Nhat, K. P. H.; Togawa, H.; Saito, K.; Iino, R.; Kato-Yamada, Y.; Nagai, T.; Noji, H. *Proc. Natl. Acad. Sci. U.S.A.* **2009**, *106*, 15651.

(20) (a) Kaelin, W. G., Jr.; Thompson, C. B. *Nature* **2010**, *465*, 562. (b) Heiden, M. G.; Cantley, L. C.; Thompson, C. B. *Science* **2009**, *324*, 1029. (c) Warburg, O. *Science* **1956**, *124*, 269.

## Conclusion

We have designed dual-emission chemosensors for nucleoside polyphosphates that are based on a new mechanism involving binding-induced recovery of FRET. These chemosensors demonstrate that binding-induced modulation of spectral overlap is a powerful strategy for the rational design of FRET-based chemosensors. The significant ratiometric change observed using these chemosensors permitted the ratiometric visualization of the ATP level inside living cells as well as the precise monitoring of two enzyme reactions involving nucleoside polyphosphates. In recent years, several protein-based luminescence biosensors for ATP based on the fusion of an ATP binding motif with fluorescent proteins have been reported.[19,21] In comparison with these biosensors, our chemosensors show relatively low sensing selectivity among polyphosphates. Nevertheless, we succeeded in using the chemosensors to image the ATP level, an indicator of cellular energy, inside cells. The easy application of our chemosensor-based approach for various cell lines is an apparent advantage over the protein biosensors reported to date, which are usually accompanied by technical difficulties such as cell-dependent control of the protein expression level and the need for a defined protein maturation time in order to obtain reliable imaging. In addition, the rather broad sensing selectivity of the present chemosensors, which are applicable to many nucleoside polyphosphates, makes these chemosensors amenable to the precise monitoring of various in vitro enzymatic reactions, such as the glycosyltransferase reaction, which would be difficult using the protein-based biosensors with high ATP specificity. On the other hand, the development of sophisticated chemosensors with high selectivity for a specific nucleoside polyphosphate is undoubtedly desirable to further facilitate the utility of chemosensors for a wider variety of bioanalytical studies. Research along these lines is currently underway in our laboratory.

## Experimental Section

**Synthesis of 6.** To a solution of **1** (240 mg, 0.38 mmol) in concentrated $H_2SO_4$ (6 mL) was added 2-chloro-*N*-(hydroxymethyl)-acetamide (528 mg, 3.04 mmol). The mixture was stirred for 30 h at room temperature (rt) and then carefully neutralized using 12 N NaOH with ice cooling. The mixture was purified by reversed-phase HPLC using the following conditions: YMC-Pack ODS-A, 20$\Phi$ × 250 mm; mobile phase, $CH_3CN$ (0.1% TFA)/$H_2O$ (0.1% TFA) = 5/95 to 50/50 (linear gradient, 90 min); flow rate, 9.999 mL/min; detection, UV (220 nm). The target fraction was collected and lyophilized to give **6** (57 mg, 20%) as a yellow solid. $^1$H NMR (400 MHz, DMSO-$d_6$): $\delta$ 8.74 (1H, s), 8.58−8.56 (4H, m), 8.21−8.19 (1H, t, $J$ = 5.2 Hz), 7.92−7.86 (4H, m), 7.55−7.49 (4H, m), 7.41−7.39 (4H, m), 7.05−7.04 (1H, d, $J$ = 2.0 Hz), 6.88 (1H, s), 6.69−6.68 (1H, d, $J$ = 2.0 Hz), 4.66 (1H, s), 4.33−4.32 (2H, d, $J$ = 4.8 Hz), 4.18 (2H, s), 4.12−4.09 (4H, m), 4.03−3.98 (8H, m). $^{13}$C NMR (100 MHz, DMSO-$d_6$): $\delta$ 165.43, 158.29, 157.95, 146.82, 139.40, 139.30, 124.03, 123.34, 58.24, 58.14, 55.30, 55.14, 42.62, 31.26. FAB-HRMS: *m*/*z* 740.2749 $[M + H]^+$.

**Synthesis of 2.** A mixture of **6** (57 mg, 0.08 mmol), **7** (60 mg, 0.15 mmol), and $K_2CO_3$ (39 mg, 0.31 mmol) in dry DMF (5.0 mL)

(21) (a) Berg, J.; Hung, Y. P.; Yellen, G. *Nat. Methods* **2009**, *6*, 161. (b) Tsuboi, T.; Lippat, J. D.; Ashcroft, F. M.; Rutter, G. A. *Proc. Natl. Acad. Sci. U.S.A.* **2004**, *101*, 76.

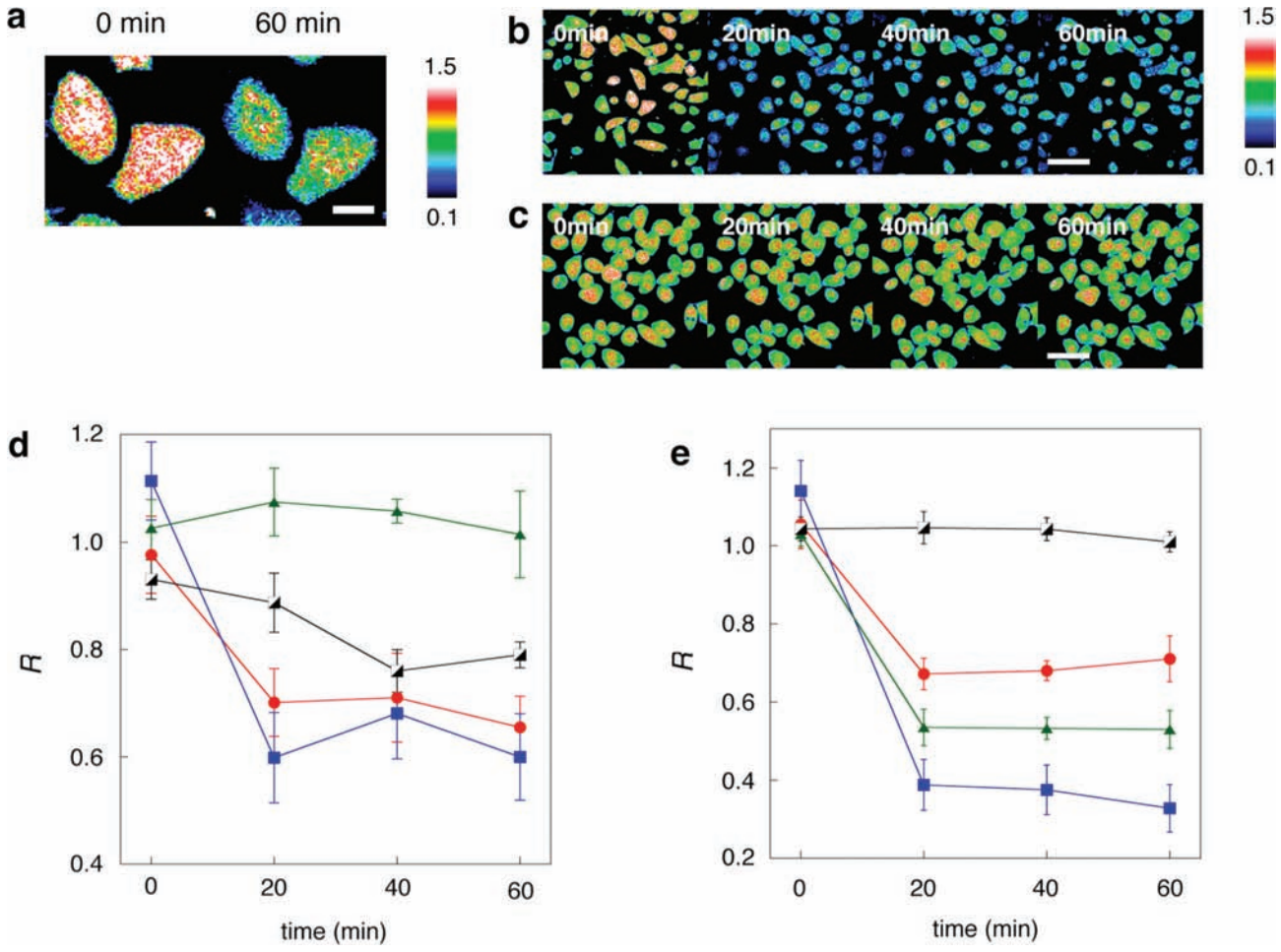


***Figure 8.*** Ratiometric analysis of living cells stained with **4**-2Zn(II). (a) Pixel-by-pixel ratio image of a HeLa cell before (0 min) and after (60 min) treatment with 20 mM 2-deoxyglucose (2-DG) and 1 mM potassium cyanide (KCN). Scale bar: 10 $\mu$m. (b, c) Time-lapse ratio imaging of HeLa cells (b) after treatment with KCN (1 mM) + 2-DG (20 mM) and (c) without the treatment. Scale bars: 50 $\mu$m. (d, e) Average time-course plots of the emission ratios of (d) HeLa cells and (e) HEK293 cells upon treatment with KCN (green line), 2-DG (red line), or KCN + 2-DG (blue line) or without the treatment (black line). *R* designates the ratio of emission intensities for the two channels [xanthene channel (530−630 nm)/coumarin channel (470−500 nm)]. Each data point was obtained from ROIs ($n$ = 5) inside the cells.

was stirred for 38 h at 50 °C. After neutralization with aqueous 10% TFA, the mixture was purified by reversed-phase HPLC using the following conditions: YMC-Pack ODS-A, 20Φ × 250 mm; mobile phase, $CH_3CN$ (0.1% TFA)/$H_2O$ (0.1% TFA) = 5/95 to 5/95 to 20/80 to 50/50 (linear gradient, 15 then 10 then 50 min); flow rate, 9.999 mL/min; detection, UV (220 nm). The fraction of interest was collected and lyophilized to give **2** (6 mg, 8%) as a yellow solid. $^1$H NMR (400 MHz, DMSO-$d_6$): $\delta$ 8.78 (1H, s), 8.58−8.56 (4H, m), 8.10 (1H, s), 7.92−7.85 (4H, m), 7.61−7.59 (1H, d, $J$ = 8.6 Hz), 7.54−7.50 (4H, m), 7.45−7.38 (4H, m), 7.08−7.07 (1H, d, $J$ = 2.2 Hz), 6.89 (1H, s), 6.85−6.82 (1H, d, $J$ = 6.4 Hz), 6.76−6.75 (1H, d, $J$ = 2.0 Hz), 6.67−6.66 (1H, d, $J$ = 2.2 Hz), 4.38−4.37 (d, 2H, $J$ = 4.6 Hz), 4.17−3.75 (m, 22H). $^{13}$C NMR (100 MHz, DMSO-$d_6$): $\delta$ 163.55, 162.57, 158.70, 158.36, 158.30, 157.62, 155.83, 147.11, 144.51, 139.10, 137.40, 130.67, 123.86, 123.81, 113.82, 110.71, 102.07, 58.32, 58.20, 55.05, 54.95, 51.82, 51.45, 31.06. FAB-HRMS: $m/z$ 978.3912 $[M + H]^+$.

**Synthesis of 2-2Zn(II).** To a solution of **2** (3.0 mg, 3.1 $\mu$mol) in distilled MeOH (3.0 mL) was added an aqueous solution of $ZnCl_2$ (6.2 $\mu$mol), and the solution was stirred for 10 min at rt. The solvent was removed to give **2**-2Zn(II) (3.6 mg, quant) as a yellow solid. FAB-HRMS: $m/z$ 1192.2601 $[M + 2Zn + H_2O + 2OH + Cl]^+$.

**Synthesis of 3.** A mixture of **6** (21 mg, 0.03 mmol), **8** (19 mg, 0.06 mmol), and $K_2CO_3$ (20 mg, 0.12 mmol) in dry DMF (1 mL) was stirred for 24 h at 50 °C. The solvent was removed by evaporation, and the residue was purified by column chromatography [$SiO_2$, $CHCl_3$/MeOH/$NH_3$(aq) = 10/1/1 to 4/1/1] and reversed-phase HPLC. HPLC conditions for purification were as follows: YMC-Pack ODS-A, 20Φ × 250 mm; mobile phase, $CH_3CN$ (0.1% TFA)/$H_2O$ (0.1% TFA) = 10/90 to 10/90 to 20/80 to 40/60 (linear gradient, 10 then 10 then 80 min); flow rate, 9.999 mL/min; detection, UV (220 nm). The fraction of interest was collected and lyophilized to give **3** (1.8 mg, 6%) as a yellow solid. $^1$H NMR (400 MHz, DMSO-$d_6$): $\delta$ 8.84 (1H, s), 8.54−8.52 (4H, m), 7.99 (1H, s), 7.84−7.78 (4H, m), 7.51−7.47 (4H, m), 7.35−7.32 (4H, m), 7.08 (1H, s), 6.88 (1H, s), 6.75−6.72 (1H, d, $J$ = 9.2 Hz), 6.66 (1H, s), 6.54−6.53 (1H, d, $J$ = 2.0 Hz), 4.36 (s, 2H), 4.13 (s, 2H), 4.06 (s, 2H), 3.93−3.89 (m, 12H), 3.49−3.41 (m, 10H) 1.14−1.10 (6H, t, $J$ = 7.2 Hz). $^{13}$C NMR (100 MHz, DMSO-$d_6$): $\delta$ 164.22, 163.60, 158.27, 157.92, 151.53, 147.47, 147.14, 138.93, 130.33, 123.80, 123.65, 123.20, 114.64, 109.53, 107.12, 96.22, 59.11, 58.30, 58.21, 57.72, 56.24, 54.91, 44.19, 12.26. FAB-HRMS: $m/z$ 1033.4735 $[M+H]^+$.

**Synthesis of 3-2Zn(II).** To a solution of **2** (0.1 mg, 0.1 $\mu$mol) in distilled MeOH (0.5 mL) was added an aqueous solution of $ZnCl_2$ (0.2 $\mu$mol), and the mixture was stirred for 10 min at rt. The solvent was removed to give **2**-2Zn(II) (0.12 mg, quant) as a yellow solid. FAB-HRMS: $m/z$ 1247.3174 $[M + 2Zn + H_2O + 2OH + Cl]^+$.

**Synthesis of 4.** To a stirred solution of **3** (47 mg, 0.046 mmol) was added 2 equiv of aqueous $ZnCl_2$ solution, and the mixture was stirred at rt for 10 min. After removal of the solvent, dry DMF (1 mL), $Ac_2O$ (377 $\mu$L, 4.0 mmol), and TEA (557 $\mu$L, 4.0 mmol)

were added to the residue. The mixture was stirred for 2 h at rt. The residue was purified by reversed-phase HPLC using the following conditions: YMC-Pack ODS-A, 20Φ × 250 mm; mobile phase, $CH_3CN$ (0.1% TFA)/$H_2O$ (0.1% TFA) = 5/95 to 5/95 to 20/80 to 50/50 (linear gradient, 15 then 10 then 50 min); flow rate, 9.999 mL/min; detection, UV (220 nm). The fraction of interest was collected and lyophilized to give **4** (3.5 mg, 7%) as a yellow solid. $^1$H NMR (400 MHz, DMSO-$d_6$): $\delta$ 8.55−8.54 (4H, m), 8.01 (1H, s), 7.90−7.85 (4H, m), 7.53−7.49 (5H, m), 7.42−7.38 (4H, m), 7.33 (1H, s), 7.31−7.30 (1H, d, $J$ = 2.0 Hz), 7.07−7.06 (1H, d, $J$ = 2.0 Hz), 6.77−6.74 (1H, d, $J$ = 6.8 Hz), 6.55−6.54 (1H, d, $J$ = 2.0 Hz), 6.22 (1H, s), 4.45−4.43 (2H, d, $J$ = 7.2 Hz), 4.38−4.31 (4H, t, $J$ = 12.0 Hz), 4.20−4.12 (4H, t, $J$ = 14.4 Hz), 4.09−4.06 (8H, m), 3.92 (2H, s), 3.48−3.43 (4H, q, $J$ = 6.8 Hz), 2.36 (3H, s), 2.30 (2, 3H), 1.13−1.10 (6H, t, $J$ = 6.8 Hz). FAB-HRMS: $m/z$ 1135.5068 $[M + H]^+$.

**Fluorescence Measurements.** Fluorescence spectra were recorded on a PerkinElmer LS55 spectrometer. Titration experiments with each phosphate anion species (Figure 3 and Table 1) were carried out with a solution (3 mL) of **2**-2Zn(II) (0.5 $\mu$M) or **3**-Zn(II) (0.5 $\mu$M) in 50 mM HEPES, 10 mM NaCl, 1 mM $MgCl_2$, pH 7.4, in a quartz cell at 25 °C. The fluorescence emission spectral change [$\lambda_{ex}$ = 341 and 414 nm for **2**-2-Zn(II) and **3**-2Zn(II), respectively] was monitored upon addition of a freshly prepared aqueous solution of the analyte with a microsyringe. The emission ratio $R = F_{xanthene}/F_{coumarin}$ was calculated from the emission intensities at the two wavelengths [$F_{525nm}/F_{454nm}$ for **2**-2Zn(II) and $F_{528nm}/F_{477nm}$ for **3**-2Zn(II)]. For evaluation of the apparent binding constant ($K_{app}$, $M^{-1}$), the fluorescence emission spectral change ($\lambda_{ex}$ = 488 nm) was measured, and the titration curve at 525 nm [**2**-2Zn(II)] or 528 nm [**3**-2Zn(II)] was analyzed using a nonlinear least-squares curve-fitting method. Abbreviations of the analytes listed in Table 1 are as follows: ATP, adenosine-5′-triphosphate; ADP, adenosine-5′-diphosphate; AMP, adenosine-5′-monophosphate; GTP, guanosine-5′-triphosphate; CTP, cytidine-5′-triphosphate; UDP, uridine-5′-diphosphate; PPi, pyrophosphoric acid; c-GMP, guanosine-3′,5′-cyclic monophosphate; c-AMP, adenosine-3′,5′-cyclic monophosphate; ADP-Gul, adenosine-5′-diphosphogulcose; UDP-Gal, uridine-5′-diphosphogalactose.

**Fluorescence Monitoring of the Glycosyl Transfer Reaction Catalyzed by $\beta$-1,4-GalT.** $\beta$-1,4-GalT was purchased from Calbiochem. An assay solution containing $\beta$-1,4-GalT (100 mU), GlcNAc (0.05, 0.1, 0.2, or 0.5 mM), and **2**-2Zn(II) (1 $\mu$M) in 100 $\mu$L of assay buffer (50 mM HEPES, 10 mM NaCl, 0.1 mM $MgCl_2$, 0.3 mM $ZnCl_2$, 0.2 mM $MnCl_2$, pH 7.2) was preincubated in a 96-well microplate at 37 °C. After addition of UDP-Gal (final concentration, 20 $\mu$M), the emission spectrum ($\lambda_{em}$ = 400−600 nm, $\lambda_{ex}$ = 341 nm) was measured using a fluorescence microplate reader (Infinite M200, TECAN). The change in the fluorescence emission ratio $R$ ($F_{525nm}/F_{454nm}$) was converted into the initial velocity ($v_0$, $\mu$M min$^{-1}$) using a calibration curve obtained from a fluorescence titration under the assay conditions. The data were analyzed using a Lineweaver−Burk plot to obtain the Michaelis constant ($K_m$, $\mu$M).

**Fluorescence Monitoring of the Phosphorylation Reaction Catalyzed by GSK-3$\beta$.** GSK-3$\beta$ was purchased from New England Biolabs. An assay solution containing ATP (25 $\mu$M), p-CREB peptide (25 $\mu$M), and **3**-2Zn(II) (10 $\mu$M) in 100 $\mu$L of assay buffer (50 mM HEPES, 10 mM $MgCl_2$, 0.1 mg/mL BSA, pH 7.2) was preincubated in a 96-well microplate at 30 °C. After addition of GSK-3$\beta$ (20, 40, 60, or 80 U), the emission spectrum ($\lambda_{em}$ = 400−600 nm, $\lambda_{ex}$ = 414 nm) was measured using a fluorescence microplate reader (Infinite M200, TECAN). The change in the fluorescence emission ratio $R$ ($F_{528nm}/F_{477nm}$) was converted into the initial velocity ($v_0$, $\mu$M min$^{-1}$) using a calibration curve obtained from a fluorescence titration under the assay conditions.

**Ratiometric Imaging in Mammalian Cells.** In a 35-mm glass-bottomed dish (MATSUNAMI), cells ($2 \times 10^5$) were cultured in high-glucose Dulbecco's Modified Eagle Medium (DMEM, 4.5 g of glucose/L) supplemented with 10% fetal bovine serum (FBS), penicillin (100 units/mL), streptomycin (100 $\mu$g/mL), and amphotericin B (250 ng/mL) under a humidified atmosphere of 5% $CO_2$ in air at 37 °C for 36 h. The cells were treated with 10 $\mu$M (final concentration) of **4**-2Zn(II) [prepared by mixing **4** with a slight excess (3 equiv) of aqueous $ZnCl_2$ solution] in HBS buffer (containing 107 mM NaCl, 6 mM KCl, 1.2 mM $MgSO_4$, 2 mM $CaCl_2$, 11.5 mM glucose, and 20 mM HEPES, pH 7.4) for 15 min at 37 °C. After replacement of the staining solution with DMEM (4.5 g of glucose/L), the cells were incubated under a humidified atmosphere of 5% $CO_2$ in air at 37 °C for 1 h. After replacing the high-glucose DMEM with glucose-free DMEM, the cells were subjected to imaging analysis using a confocal scanning laser microscope (Olympus, FLUOVIEW FV1000) under a continuous supply of 5% $CO_2$ in air while the temperature was maintained at 37 °C. The fluorescence images were obtained by excitation at 458 nm and simultaneous detection with two different channels (channel 1, 470−500 nm for the coumarin emission; channel 2, 530−630 nm for the xanthene emission). Ratio image analyses were performed using FV10-ASW (version 1.6).

**Supporting Information Available:** Detailed synthetic procedures and compound characterizations, fluorescence titration and Job's plot of the chemosensors with ATP, calculation of the FRET efficiency, pH-dependent fluorescence profiles of the chemosensors, and selected data from the ratiometric imaging in mammalian cells. This material is available free of charge via the Internet at http://pubs.acs.org.

JA103615Z